Dijet azimuthal decorrelations at the LHC in the parton Reggeization approach

M.A. Nefedov*

Samara State University, Ac. Pavlov, 1, 443011 Samara, Russia

V.A. Saleev† and A.V. Shipilova‡

Samara State University, Ac. Pavlov, 1, 443011 Samara, Russia and

II. Institut für Theoretische Physik, Universität Hamburg,

Luruper Chaussee 149, 22761 Hamburg, Germany

Abstract

We study inclusive dijet azimuthal decorrelations in proton-proton collisions at the CERN LHC invoking the hypothesis of parton Reggeization in $t-$channel exchanges at high energies. In the parton Reggeization approach, the main contribution to the azimuthal angle difference between the two most energetic jets is due to the Reggeon-Reggeon-Particle-Particle scattering, when the fusion of two Reggeized gluons into a pair of Yang-Mills gluons dominates. Using a high-energy factorization scheme with the Kimber-Martin-Ryskin unintegrated parton distribution functions and the Fadin-Lipatov effective vertices we obtain good agreement of our calculations with recent measurements by the ATLAS and CMS Collaborations at the CERN LHC.

PACS numbers: 12.38.Bx, 12.39.St, 13.87.Ce

*Electronic address: nefedovma@gmail.com

†Electronic address: saleev@samsu.ru

‡Electronic address: alexshipilova@samsu.ru

I. INTRODUCTION

The production of large transverse-momentum (p_T) hadron jets at the high-energy colliders, like the Tevatron and the LHC, is reasonably considered as an important source of information about dynamics of parton-parton interactions at small distances and parton distribution functions (PDF), and as a probe to test perturbative quantum chromodynamics (pQCD) [1]. The measurements of decorrelations in the azimuthal angle between the two most energetic jets, $\Delta\varphi$, as a function of number of produced jets, give the chance to separate directly leading order (LO) and next-to-leading orders (NLO) contributions in the strong coupling constant α_s. Furthermore, a precise understanding of the physics of events with large azimuthal decorrelations is essential for the search of new physical phenomena with dijet signatures by the CMS [2] and ATLAS [3] detectors at the LHC.

The total collision energies, $\sqrt{S} = 7$ TeV or 14 TeV at the LHC, sufficiently exceed the transverse momenta of identified jets ($0.1 < p_T < 1.3$ TeV). The recent theoretical studies of single jet production at very high energy show the dominance of the multi-Regge final states in the inclusive production cross sections [4]. In other words, in the high-energy regime the contribution of partonic subprocesses involving $t-$channel parton exchanges become dominant. Then the transverse momenta of the incoming partons and their off-shell properties can no longer be neglected, and we deal with QCD-scattering amplitudes with Reggeized $t-$channel partons. As it has been shown by Lipatov and co-authors, Reggeized gluons and quarks are the appropriate gauge-invariant degrees of freedom of high-energy pQCD. In the practical applications, the use of Reggeized $t-$channel exchanges is justified by the dominance of the so-called multi-Regge final states in inelastic collisions of high-energy hadrons.

The parton Reggeization approach [5, 6] is based on an effective quantum field theory implemented with the non-Abelian gauge-invariant action which includes fields of Reggeized gluons [7] and Reggeized quarks [8]. Recently, this approach was successfully applied to interpret the p_T-spectra of inclusive production of single jet [4], prompt-photon [9, 10], Drell-Yan lepton pairs [11] and bottom-flavored jets [12, 13] at the Tevatron and LHC. The single jet production is dominated by the multi-Regge kinematics (MRK), when only a jet with a highest transverse momentum (leading jet) is produced in the central rapidity region, being strongly separated in rapidity from other particles. If the same situation is realized for two or more the most energetic jets, then quasi-multi-Regge kinematics (QMRK) is at

work.

In the present paper we extend our analysis of inclusive single jet production at the LHC based on the parton Reggeization approach onto a case of dijet production, and study azimuthal decorrelations between the two central jets with the largest transverse momenta according to the measurements implemented by the CMS and ATLAS Collaborations [2, 3].

This paper is organized as follows: In Sec. II, the parton Reggeization approach is briefly reviewed. We write down relevant Reggeon-Reggeon-Particle-Particle effective vertices, effective amplitudes, squared matrix elements and differential cross sections. In Sec. III, we present the results of our calculations for two-jet azimuthal decorrelation spectra and perform a comparison with corresponding experimental data from the CERN LHC at $\sqrt{S} = 7$ TeV. Sec. IV contains our conclusions.

II. DIJET PRODUCTION IN QMRK

In the high-energy Regge limit, when the collision energy is very high but the transverse momenta of produced jets are fixed by the condition $\sqrt{S} >> p_T >> \Lambda_{QCD}$, the high-energy (uncollinear) factorization works well instead of collinear parton model. In this case, the Balitsky-Fadin-Kuraev-Lipatov (BFKL) QCD-evolution of unintegrated PDFs [14] can be more adequate approximation than the Dokshtser-Gribov-Lipatov-Altarelli-Parisi (DGLAP) QCD-evolution of collinear PDFs [15]. It means, that we need to consider the processes with strong ordering in rapidity at the MRK or QMRK conditions. We identify final-state jets and final-state partons, and consider production of two partons in the central region of rapidity, assuming that there are no any other partons with the same rapidity. To the LO in the parton Reggeization approach we have the following partonic subprocesses, which

describe production of two central jets in proton-proton collisions:

$$R + R \to g + g, \tag{1}$$

$$R + R \to q + \bar{q}, \tag{2}$$

$$Q + R \to q + g, \tag{3}$$

$$Q + Q \to q + q, \tag{4}$$

$$Q + Q' \to q + q', \tag{5}$$

$$Q + \bar{Q} \to q + \bar{q}, \tag{6}$$

$$Q + \bar{Q} \to q' + \bar{q}', \tag{7}$$

$$Q + \bar{Q} \to g + g, \tag{8}$$

where R is a Reggeized gluon, Q is a Reggeized quark, g is a Yang-Mills gluon, q is an ordinary quark, q and q' denote quarks of different flavors. Working in the center-of-mass (c.m.) frame, we write the four-momenta of the incoming protons as $P^\mu_{1,2} = (\sqrt{S}/2)(1, 0, 0, \pm 1)$ and those of the Reggeized partons as $q^\mu_i = x_i P^\mu_i + q^\mu_{iT}$ $(i = 1, 2)$, where x_i are longitudinal momentum fractions and $q^\mu_{iT} = (0, \mathbf{q}_{iT}, 0)$, with $\mathbf{q}_{iT}$ being transverse two-momenta, and we define $t_i = -q^2_{iT} = \mathbf{q}^2_{iT}$. The final partons have four-momenta $k_{1,2}$ and they are on-shell and massless $k^2_1 = k^2_2 = 0$.

The effective gauge invariant amplitudes for the above mentioned subprocesses (1)-(8) can be obtained using the effective Feynman rules from Refs. [7, 8, 16]. As usual, we introduce the light-cone vectors $n^+ = 2P_2/\sqrt{S}$ and $n^- = 2P_1/\sqrt{S}$, and define $k^\pm = k \cdot n^\pm$ for any four-vector k^μ. Than we determine effective vertices:

$$\Gamma^{(+-)}_\mu(q_1, q_2) \;=\; 2\left[\left(q_1^+ + \frac{q_1^2}{q_2^-}\right) n^-_\mu - \left(q_2^- + \frac{q_2^2}{q_1^+}\right) n^+_\mu + (q_2 - q_1)_\mu\right], \tag{9}$$

$$\gamma^\pm_\mu(q, p) \;=\; \gamma_\mu + \hat{q}\frac{n^\pm_\mu}{p^\pm}, \tag{10}$$

$$\gamma^{(+-)}_\mu(q_1, q_2) \;=\; \gamma_\mu - \hat{q}_1\frac{n^-_\mu}{q_2^-} - \hat{q}_2\frac{n^+_\mu}{q_1^+}, \tag{11}$$

$$\begin{aligned}
\Gamma^{\mu\nu+}(q_1, q_2) \;&=\; 2q_1^+ g^{\mu\nu} - (n^+)^\mu(q_1 - q_2)^\nu - (n^+)^\nu(q_1 + 2q_2)^\mu + \frac{t_2}{q_1^+}(n^+)^\mu(n^+)^\nu, \\
\Gamma^{\mu\nu-}(q_1, q_2) \;&=\; 2q_2^- g^{\mu\nu} + (n^-)^\mu(q_1 - q_2)^\nu - (n^-)^\nu(q_2 + 2q_1)^\mu + \frac{t_1}{q_2^-}(n^-)^\mu(n^-)^\nu,
\end{aligned} \tag{12}$$

and the triple-gluon vertex

$$\gamma_{\mu\nu\sigma}(q, p) \;=\; (q - p)_\sigma g_{\mu\nu} - (p + 2q)_\mu g_{\nu\sigma} + (2p + q)_\nu g_{\mu\sigma}. \tag{13}$$

Finally, we can write the effective vertices for relevant subprocesses as follows:

$$C^{gg,\ cd,\ \mu\nu}_{RR,ab}(q_1,q_2,k_1,k_2) \ = \ g_s^2\frac{q_1^+q_2^-}{4\sqrt{t_1t_2}}\Big(T_1s^{-1}\Gamma^{(+-)_\sigma}(q_1,q_2)\gamma_{\mu\nu\sigma}(-k_1,-k_2)+$$
$$+\ T_3t^{-1}\Gamma^{\sigma\mu-}(q_1,k_1-q_1)\Gamma^{\sigma\nu+}(k_2-q_2,q_2)-$$
$$-\ T_2u^{-1}\Gamma^{\sigma\nu-}(q_1,k_2-q_1)\Gamma^{\sigma\mu+}(k_1-q_2,q_2)-$$
$$-\ T_1\big(n_\mu^-n_\nu^+-n_\nu^-n_\mu^+\big)-T_2\big(2g_{\mu\nu}-n_\mu^-n_\nu^+\big)-T_3\big(-2g_{\mu\nu}+n_\nu^-n_\mu^+\big)+$$
$$+\ \Delta^{\mu\nu+}(q_1,q_2,k_1,k_2)+\Delta^{\mu\nu-}(q_1,q_2,k_1,k_2)\Big), \qquad (14)$$

where

$$T_1=f_{cdr}f_{abr},\quad T_2=f_{dar}f_{cbr},\quad T_3=f_{acr}f_{dbr},\quad T_1+T_2+T_3=0,$$
$$\Delta^{\mu\nu+}(q_1,q_2,k_1,k_2)=2t_2n_\mu^+n_\nu^+\left(\frac{T_3}{k_2^+q_1^+}-\frac{T_2}{k_1^+q_1^+}\right),$$
$$\Delta^{\mu\nu-}(q_1,q_2,k_1,k_2)=2t_1n_\mu^-n_\nu^-\left(\frac{T_3}{k_1^-q_2^-}-\frac{T_2}{k_2^-q_2^-}\right),$$

f^{abc} are structure constants of color gauge group SU(3), $g_s^2=4\pi\alpha_s$, and α_s is a strong-coupling constant.

$$C^{q\bar q,\ }_{RR,\ ab}(q_1,q_2,k_1,k_2) \ = \ g_s^2\frac{q_1^+q_2^-}{4\sqrt{t_1t_2}}\bar U(k_1)\left(-s^{-1}[T^a,T^b]\gamma^\sigma\Gamma^{(+-)}_\sigma(q_1,q_2)+\right.$$
$$\left.+\ t^{-1}T^aT^b\gamma^-(\hat k_1-\hat q_1)\gamma^++u^{-1}T^bT^a\gamma^+(\hat k_1-\hat q_2)\gamma^-\right)V(k_2), \qquad (15)$$

$$C^{qg,\ b,\ \mu}_{QR,\ a}(q_1,q_2,k_1,k_2) \ = \ \frac{1}{2}g_s^2\frac{q_2^-}{2\sqrt{t_2}}\bar U(k_1)\Big[\gamma^{(-)}_\sigma(q_1,k_1-q_1)t^{-1}\big(\gamma_{\mu\nu\sigma}(k_2,-q_2)n_\nu^++t_2\frac{n_\mu^+n_\sigma^+}{k_2^+}\big)\times$$
$$\times\ \big[T^a,T^b\big]-\gamma^+(\hat q_1-\hat k_2)^{-1}\gamma^{(-)}_\mu(q_1,-k_2)T^aT^b-$$
$$-\ \gamma_\mu(\hat q_1+\hat q_2)^{-1}\gamma^{(-)}_\sigma(q_1,q_2)n_\sigma^+T^bT^a+\frac{2\hat q_1n_\mu^-}{k_1^-}\left(\frac{T^aT^b}{k_2^-}-\frac{T^bT^a}{q_2^-}\right)\Big], \qquad (16)$$

$$C^{qq}_{QQ}(q_1,q_2,k_1,k_2) \ = \ g_s^2\left(t^{-1}\bar U(k_2)\gamma^{(+)}_\sigma(q_2,k_2-q_2)T^c\otimes\bar U(k_1)\gamma^{(-)}_\sigma(q_1,k_1-q_1)T^c-\right.$$
$$\left.-\ u^{-1}\bar U(k_1)\gamma^{(+)}_\sigma(q_2,k_1-q_2)T^c\otimes\bar U(k_2)\gamma^{(-)}_\sigma(q_1,k_2-q_1)T^c\right), \qquad (17)$$

$$C^{qq'}_{QQ'}(q_1,q_2,k_1,k_2)=g_s^2t^{-1}\bar U(k_2)\gamma^{(+)}_\sigma(q_2,k_2-q_2)T^c\otimes\bar U(k_1)\gamma^{(-)}_\sigma(q_1,k_1-q_1)T^c, \qquad (18)$$

$$C^{q\bar q}_{Q\bar Q}(q_1,q_2,k_1,k_2) \ = \ g_s^2\left(s^{-1}\bar U(k_1)\gamma_\sigma T^cV(k_2)\otimes\gamma^{(+-)}_\sigma(q_1,q_2)T^c+\right.$$
$$\left.+\ t^{-1}\bar U(k_1)\gamma^{(+)}_\sigma(q_2,k_2-q_2)T^c\otimes\gamma^{(-)}_\sigma(q_1,k_1-q_1)T^cV(k_2)\right), \qquad (19)$$

$$C_{Q\bar{Q}}^{q'\bar{q}'}(q_1,q_2,k_1,k_2) = g_s^2 s^{-1}\bar{U}(k_1)\gamma_\sigma T^c V(k_2)\otimes\gamma_\sigma^{(+-)}(q_1,q_2)T^c, \tag{20}$$

$$\begin{aligned} C_{Q\bar{Q}}^{gg,\ ab,\ \mu\nu}(q_1,q_2,k_1,k_2) \ &= \ -g_s^2\Big(\gamma_\nu^{(+)}(q_2,-k_2)(\hat{k}_2-\hat{q}_2)^{-1}\gamma_\mu^{(-)}(q_1,-k_1)T^bT^a + \\ &+ \ \gamma_\nu^{(+)}(q_2,-k_1)(\hat{k}_1-\hat{q}_2)^{-1}\gamma_\mu^{(-)}(q_1,-k_2)T^aT^b + \\ &+ \ \gamma_{\mu\nu\sigma}(-k_1,-k_2)s^{-1}\gamma_\sigma^{(+-)}(q_1,q_2)[T^a,T^b]+\Delta_{\mu\nu}^{ab}(q_1,q_2)\Big), \end{aligned} \tag{21}$$

where

$$\Delta_{\mu\nu}^{ab}(q_1,q_2) = \frac{\hat{q}_1 n_\mu^- n_\nu^-}{q_2^-}\left(\frac{T^aT^b}{k_2^-}+\frac{T^bT^a}{k_1^-}\right) - \frac{\hat{q}_2 n_\mu^+ n_\nu^+}{q_1^+}\left(\frac{T^aT^b}{k_1^+}+\frac{T^bT^a}{k_2^+}\right).$$

The effective amplitudes of the subprocesses (1)-(8) are straightforwardly found from Eqs. (14)-(21). In case of gluon production amplitudes we convolute effective vertices with final gluon polarization vectors $\epsilon_\mu^a(k_1)$ and $\epsilon_\nu^b(k_2)$. In case of amplitudes with the initial-state Reggeized quark Q and antiquark $\bar{Q}$, we take their spinors as $U(x_1P_1)$ and $V(x_2P_2)$ [8]. In such a way, omitting the color indices, we obtain

$$\mathcal{M}(RR\to gg) = \epsilon_\mu(k_1)\epsilon_\nu(k_2)C_{RR}^{gg,\ \mu\nu}(q_1,q_2,k_1,k_2), \tag{22}$$

$$\mathcal{M}(RR\to q\bar{q}) = C_{RR}^{q\bar{q}}(q_1,q_2,k_1,k_2), \tag{23}$$

$$\mathcal{M}(QR\to qg) = \epsilon_\mu(k_2)C_{QR}^{qg,\ \mu}(q_1,q_2,k_1,k_2)U(x_1P_1), \tag{24}$$

$$\mathcal{M}(QQ\to qq) = C_{QQ}^{qq}(q_1,q_2,k_1,k_2)U(x_1P_1)\otimes U(x_2P_2), \tag{25}$$

$$\mathcal{M}(QQ'\to qq') = C_{QQ'}^{qq'}(q_1,q_2,k_1,k_2)U(x_1P_1)\otimes U'(x_2P_2), \tag{26}$$

$$\mathcal{M}(Q\bar{Q}\to q\bar{q}) = \bar{V}(x_2P_2)C_{Q\bar{Q}}^{q\bar{q}}(q_1,q_2,k_1,k_2)U(x_1P_1), \tag{27}$$

$$\mathcal{M}(Q\bar{Q}\to q'\bar{q}') = \bar{V}(x_2P_2)C_{Q\bar{Q}}^{q'\bar{q}'}(q_1,q_2,k_1,k_2)U(x_1P_1), \tag{28}$$

$$\mathcal{M}(Q\bar{Q}\to gg) = \epsilon_\mu(k_1)\epsilon_\nu(k_2)\bar{V}(x_2P_2)C_{Q\bar{Q}}^{gg,\ \mu\nu}(q_1,q_2,k_1,k_2)U(x_1P_1). \tag{29}$$

To calculate dijet production cross section we have found squared amplitudes $\overline{|\mathcal{M}|^2}$ of above mentioned subprocesses (1)-(8), where the bar indicates average (summation) over

initial-state (final-state) spins and colors. The results are written as functions of the Mandelstam variables $s = (q_1 + q_2)^2$, $t = (q_1 - k_1)^2$, $u = (q_1 - k_2)^2$, and invariant Sudakov variables $a_1 = 2k_1 \cdot P_2/S$, $a_2 = 2k_2 \cdot P_2/S$, $b_1 = 2k_1 \cdot P_1/S$, $b_2 = 2k_2 \cdot P_1/S$. The four-momenta of final-state partons can be introduced as a sum of longitudinal and transverse parts: $k_1 = a_1 P_1 + b_1 P_2 + k_{1T}$, $k_2 = a_2 P_1 + b_2 P_2 + k_{2T}$. Applying a four-momentum conservation law one can find $x_1 = a_1 + a_2$, $x_2 = b_1 + b_2$ and $q_{1T} + q_{2T} = k_{1T} + k_{2T}$. In general case, the squared amplitudes can be written in the form

$$\overline{|\mathcal{M}|^2} = \pi^2 \alpha_S^2 A \sum_{n=0}^{4} W_n S^n, \tag{30}$$

where A and W_n are process-dependent functions of variables $s, t, u, a_1, a_2, b_1, b_2, t_1, t_2, S$. The exact analytical formulas for A and W_n are presented in Sec. Appendix. Our definition of the Reggeized amplitudes satisfy evident normalization to the QCD-amplitudes of the collinear parton model:

$$\lim_{t_1,t_2 \to 0} \int \frac{d\varphi_1}{2\pi} \int \frac{d\varphi_2}{2\pi} \overline{|\mathcal{M}(t_1, t_2, \varphi_1, \varphi_2)|^2} = \overline{|\mathcal{M}_{PM}|^2}. \tag{31}$$

This condition has been checked for all squared matrix elements $\overline{|\mathcal{M}|^2}$ presented in Sec. Appendix.

Here we present an analytic formula for differential cross section for dijet production process via the subprocess (1), which gives a main contribution, and take in mind that other contributions can be written in the same manner. So, according to the high-energy factorization formalism, the proton-proton production cross section is obtained by the convolution of squared matrix element $\overline{|\mathcal{M}(RR \to gg)|^2}$ with the unintegrated Reggeized gluon PDFs $\Phi_g^p(x_{1,2}, t_{1,2}, \mu^2)$ at the factorization scale μ [19]:

$$\frac{d\sigma(pp \to ggX)}{dk_{1T} dy_1 dk_{2T} dy_2 d\Delta\varphi} = \frac{k_{1T} k_{2T}}{16\pi^3} \int dt_1 \int d\phi_1 \Phi_g^p(x_1, t_1, \mu^2) \Phi_g^p(x_2, t_2, \mu^2) \frac{\overline{|\mathcal{M}(RR \to gg)|^2}}{(x_1 x_2 S)^2}, \tag{32}$$

where $k_{1,2T}$ and $y_{1,2}$ are final gluon transverse momenta and rapidities, respectively, and $\Delta\varphi$ is an azimuthal angle enclosed between the vectors $\vec{k}_{1T}$ and $\vec{k}_{2T}$,

$$x_1 = (k_1^0 + k_2^0 + k_1^z + k_2^z)/\sqrt{S}, \quad x_2 = (k_1^0 + k_2^0 - k_1^z - k_2^z)/\sqrt{S},$$

$$k_{1,2}^0 = k_{1,2T} \cosh(y_{1,2}), \quad k_{1,2}^z = k_{1,2T} \sinh(y_{1,2}).$$

Throughout our analysis the renormalization and factorization scales are identified and chosen to be $\mu = \xi k_{1T}$, where k_{1T} is a the transverse momentum of the leading jet ($k_{1T} > k_{2T}$)

and ξ is varied between 1/2 and 2 about its default value 1 to estimate the theoretical uncertainty due to the freedom in the choice of scales. The resulting errors are indicated as shaded bands in the figures.

The unintegrated PDFs $\Phi_g^p(x,t,\mu^2)$ are related to their collinear counterparts $f_g^p(x,\mu^2)$ by the normalization condition

$$x f_g^p(x,\mu^2) = \int^{\mu^2} dt\, \Phi_g^p(x,t,\mu^2), \tag{33}$$

which furnishes a correct transition from formulas in parton Reggeization approach to those in the collinear parton model. In our numerical analysis, we adopt the prescription proposed by Kimber, Martin, and Ryskin (KMR) [17] to obtain the unintegrated gluon and quark PDFs of the proton from the conventional integrated ones. As input for these procedures, we use the LO set of the Martin-Roberts-Stirling-Thorne (MRST) [18] proton PDFs as our default.

III. RESULTS

Recently, CMS [2] and ATLAS [3] Collaborations have measured azimuthal decorrelations between the two central jets with the highest transverse momenta (leading jets) in proton-proton collisions at $\sqrt{S} = 7$ TeV. The kinematic domains of jets transverse momenta and rapidities in these experiments are slightly different. The CMS Collaboration selected two leading jets each with $p_T > 30$ GeV and rapidity $|y| < 1.1$ and collected data into five mutually exclusive regions, which are based on the p_T^{max} in the event: $80 < p_T^{max} < 110$ GeV, $110 < p_T^{max} < 140$ GeV, $140 < p_T^{max} < 200$ GeV, $200 < p_T^{max} < 300$ GeV, and $p_T^{max} > 300$ GeV. The ATLAS Collaboration selected two leading jets each with $p_T > 100$ GeV and rapidity $|y| < 0.8$ and collected data into nine regions: $100 < p_T^{max} < 160$ GeV, $160 < p_T^{max} < 210$ GeV, $210 < p_T^{max} < 260$ GeV, $260 < p_T^{max} < 310$ GeV, $310 < p_T^{max} < 400$ GeV, $400 < p_T^{max} < 500$ GeV, $500 < p_T^{max} < 600$ GeV, $600 < p_T^{max} < 800$ GeV, and $p_T^{max} > 800$ GeV. The measurements are presented for the region of $\pi/2 < \Delta\varphi < \pi$ as normalized distributions

$$F(\Delta\varphi) = \frac{1}{\sigma} \times \left(\frac{d\sigma}{d\Delta\varphi}\right), \tag{34}$$

where

$$\sigma = \int_{\pi/2}^{\pi} \left(\frac{d\sigma}{d\Delta\varphi}\right) d\Delta\varphi.$$

Additionally, the ATLAS Collaboration presented the $\Delta\varphi$ distribution of events with ≥ 2, ≥ 3, ≥ 4, and ≥ 5 jets with $p_T > 100$ GeV and $|y| < 0.8$ for the leading jets and $|y| < 2.8$ for all other jets.

The theoretical expectations based on the collinear parton model for $\Delta\varphi$ distributions include pQCD calculation in NLO (α_S^4) for the three-parton final states and LO (α_S^4) for the four-parton final states [20]. As it has been demonstrated in Refs. [2, 3], these calculations describe data in the region of $2\pi/3 < \Delta\varphi < \pi$ and overestimate data at $\Delta\varphi < 2\pi/3$. The agreement of parton model calculations with data can be achieved using the Monte Carlo event generators (MC), such as: PYTHIA [21], HERWIG++ and MADGRAPH [22]. These parton-level generators include NLO pQCD matrix elements, different collinear PDFs, effects of hadronization and the initial-state parton shower radiation (ISR). The last one is very important to simulate events at $\Delta\varphi < 2\pi/3$ but it is needed to introduce a new theoretically unknown parameter k_{ISR}, which can be fixed phenomenologically only.

To obtain a distribution $F(\Delta\phi)$ in the frameworks of the parton Reggeization approach, we perform an integration of the differential cross section (32) over the final-state parton transverse momenta k_{1T} and k_{2T}, as well as over the rapidities y_1 and y_2 in the intervals defined by the experiment. We take into account contributions of all necessary subprocesses (1)-(8), where quark flavors are taken $q = u, d, s$ for initial-state and final-state quarks. The upper limit for the squares of Reggeized gluons transverse momenta t_1 and t_2 should be truncated by the condition $t_1, t_2 < k_{2T}^2$, where k_{2T} is a smaller transverse momentum of a jet from the pair of two leading jets. The above-mentioned condition arises from the constraints of LHC experiment: one can measure an azimuthal angle between the two most energetic jets $\Delta\varphi$ but it is impossible to separate final-state partons produced in the hard parton scattering phase from the ones generated during QCD-evolution of PDFs. The BFKL evolution suggests a strong ordering in rapidity but transverse momenta of partons in the QCD-ladder keep similar values. It means, that the transverse momenta of partons generated in the initial-state evolution, described via the unintegrated PDF must be smaller than transverse momenta of both measured leading jets.

The CMS measurements [2] of $F(\Delta\phi)$ distributions for the two most energetic jets are shown in Fig. 1. A comparison of the LO parton Reggeization approach predictions with the data demonstrates a nice agreement in the region of $\Delta\varphi \geq 3\pi/4$. As $\Delta\varphi$ decreases from $3\pi/4$ to $\pi/2$, the theoretical expectations tend to underestimate data more and more, up to a factor 5 at the $80 < p_T^{max} < 110$ GeV and a factor 2 at the $200 < p_T^{max} < 300$ GeV. This difference follows from our theoretical approximation: we take into account only two-jet production subprocesses in the QMRK, like the $RR \to gg$. However, at $\Delta\varphi \simeq \pi/2$, the contribution of three-jet production subprocess should be important. One can find, the difference becomes smaller with growing of p_T^{max}, because the situation when transverse momentum of leading jet is compensated by the one energetic jet in opposite direction is more probable than the such compensation by two or more jets.

Our observations are confirmed in Fig. 2, where the data from ATLAS Collaboration [3] are compared with theoretical predictions. We see, the disagreements between our predictions and ATLAS data are smaller than in the case of CMS data. This fact can be explained by the difference of the choice of low-p_T cut for both Collaborations: CMS measurements have been performed for jet production with $p_T > 30$ GeV, and ATLAS measurements – with $p_T > 110$ GeV.

Certainly, the precise comparison of theoretical predictions in the LO parton Reggeization approach should be made when we separate only the two-jet production in the central rapidity region. In fact, the data include multi-jet production contribution. The ATLAS Collaboration presents the $\Delta\varphi-$distributions for different number of final-state jets (see Fig. 1 in Ref. [3]). Using these data, we can extract $F(\Delta\varphi)$ for two-jet production only, as a difference between number of events: $n(2) = n(\geq 2) - n(\geq 3)$ or $\sigma(2)F(\Delta\varphi, 2) = \sigma(\geq 2)F(\Delta\varphi, \geq 2) - \sigma(\geq 3)F(\Delta\varphi, \geq 3)$. The original ATLAS data for $F(\Delta\varphi, \geq 2)$ and extracted data for $F(\Delta\varphi, 2)$ are shown in Fig. 3 for the kinematic domain of $p_T^{max} > 100$ GeV and $|y| < 0.8$. We see, the theoretical prediction nicely agrees with data for $F(\Delta\varphi, 2)$ distribution. So, if the last one would be extracted for different regions of p_T^{max}, we can make a more precise comparison of our predictions with experimental data.

Summarizing results of a present analysis for dijet production at the LHC and our previous study of $b\bar{b}-$pair production at the Tevatron and LHC [12, 13], we find a strong difference of theoretical interpretation of azimuthal decorrelation between leading and subleading jets, in the collinear parton model and in the parton Reggeization approach. In the first case, an

azimuthal decorrelation at different values of $\Delta\varphi$ is provided by hard $2 \to 3$ ($3\pi/4 < \Delta\varphi < \pi$), $2 \to 4$ ($\pi/2 < \Delta\varphi < 3\pi/4$) partonic subprocesses, correspondingly. The explanation of data in the region of $\Delta\varphi < \pi/2$ in the framework of collinear parton model becomes possible only because of initial-state radiation and hadronization effects, and an agreement of theory expectations and data is achieved using MC generators only.

Oppositely, in the parton Reggeization approach, the azimuthal decorrelation is explained by the coherent parton emission during the QCD-evolution, which is described by the transverse-momentum dependent PDFs of Reggeized partons. Already in the LO approximation, at the level of $2 \to 2$ subprocesses with Reggeized partons, we can account the main part of decorrelation effect in dijet production, and we obtain a full description of data in $b\bar{b}-$pair production.

IV. CONCLUSIONS

This good description of dijet azimuthal decorrelations is achieved in the LO parton Reggeization approach, without any ad-hoc adjustments of input parameters. By contrast, in the collinear parton model, such a degree of agreement calls for NLO and NNLO corrections and complementary initial-state radiation effects and ad-hoc nonperturbative transverse momenta of partons. In conclusion, the parton Reggeization approach has once again proven to be a powerful tool for the theoretical description of QCD processes induced by Reggeized partons in the high-energy limit. As it was shown by the recent studies [23], the one-loop calculations in this formalism lead the results for the NLO effective vertices, consistent with the earlier calculations based on unitarity relations [24]. These results open a possibility to extend the calculations of hard processes in the parton Reggeization approach to the complete-NLO level.

Acknowledgements

We are grateful to B. A. Kniehl, E. A. Kuraev, L. N. Lipatov and N. N. Nikolaev for useful discussions. The work of V. S. was supported by the Ministry for Science and Education of the Russian Federation under Contract No. 14.B37.21.1182. The work of M. N. and A. S. was supported in part by the Russian Foundation for Basic Research under Grant 12-02-

31701-mol-a. The work of M. N. is supported also by the Grant of the Graduate Students Stipend Program of the Dynasty Foundation. The work of A. S. was also supported in part by Michail Lomonosov Grant No. A/11/76586, jointly funded by the German Academic Exchange Service DAAD and the Ministry of Science and Education of Russian Federation. V.S. and A.S. are kindly grateful to B. A. Kniehl for the hospitality and the computational resources provided during their visits. V.S. and A.S. express gratitude to E. Kader for her help in technical aspects during the preparation of this paper.

---

[1] B.L. Ioffe, V.S. Fadin and L.N. Lipatov, Quantum chromodynamics. Perturbative and non-perturbative aspects. Cambridge University Press, 2010, Cambridge, UK; D. Green, High p_T physics at hadron colliders. Cambridge University Press, 2005, Cambridge, UK.

[2] CMS Collaboration, V. Khachatryan at al., Phys. Rev. Lett. **106**, 122003 (2011).

[3] ATLAS Collaboration, G. Aad et al., Phys. Rev. Lett. **106**, 172002 (2011).

[4] B. A. Kniehl, V. A. Saleev, A. V. Shipilova, E. V. Yatsenko, Phys. Rev. **D84** , 074017 (2011).

[5] V. S. Fadin and L. N. Lipatov, Nucl. Phys. **B406**, 259 (1993); **B477**, 767 (1996).

[6] V. S. Fadin and V. E. Sherman, JETP Lett. **23**, 599 (1976); JETP **45**, 861 (1977).

[7] L. N. Lipatov, Nucl. Phys. **B452**, 369 (1995).

[8] L. N. Lipatov and M. I. Vyazovsky, Nucl. Phys. **B597**, 399 (2001).

[9] V. A. Saleev, Phys. Rev. D **78**, 034033 (2008).

[10] V. A. Saleev, Phys. Rev. D **78**, 114031 (2008).

[11] M.A. Nefedov, N.N. Nikolaev, and V.A. Saleev, Phys. Rev. D **87**, 014022 (2013).

[12] B. A. Kniehl, A. V. Shipilova, and V. A. Saleev, Phys. Rev. D **81**, 094010 (2010).

[13] V.A. Saleev, A.V. Shipilova, Phys. Rev. D**86**, 034032 (2012).

[14] L. N. Lipatov, Sov. J. Nucl. Phys. **23**, 338 (1976) [Yad. Fiz. **23**, 642 (1976)]; E. A. Kuraev, L. N. Lipatov, and V. S. Fadin, Sov. Phys. JETP **44**, 443 (1976) [Zh. Eksp. Teor. Fiz. **71**, 840 (1976)]; Sov. Phys. JETP **45**, 199 (1977) [Zh. Eksp. Teor. Fiz. **72**, 377 (1977)]; I. I. Balitsky and L. N. Lipatov, Sov. J. Nucl. Phys. **28**, 822 (1978) [Yad. Fiz. **28**, 1597 (1978)]; Sov. Phys. JETP **63**, 904 (1986) [Zh. Eksp. Teor. Fiz. **90**, 1536 (1986)].

[15] V. N. Gribov and L. N. Lipatov, Sov. J. Nucl. Phys. **15**, 438 (1972) [Yad. Fiz. **15**, 781 (1972)]; Yu. L. Dokshitzer, Sov. Phys. JETP **46**, 641 (1977) [Zh. Eksp. Teor. Fiz. **73**, 1216 (1977)];

G. Altarelli and G. Parisi, Nucl. Phys. **B126**, 298 (1977).

[16] E. N. Antonov, L. N. Lipatov, E. A. Kuraev, and I. O. Cherednikov, Nucl. Phys. **B721**, 111 (2005).

[17] M. A. Kimber, A. D. Martin, and M. G. Ryskin, Eur. Phys. J. C **12**, 655 (2000); Phys. Rev. D **63**, 114027 (2001); G. Watt, A. D. Martin, and M. G. Ryskin, Eur. Phys. J. C **31**, 73 (2003).

[18] A. D. Martin, W. J. Stirling, R. S. Thorne, Phys. Lett. **B636** 259 (2006).

[19] V.A. Saleev, Phys. Rev. D **80**, 114016 (2009).

[20] Z. Nagy, Phys. Rev. Lett. **88**, 122003 (2002).

[21] T. Sjostrand, S. Mrenna, and P. Skands, Comput. Phys. Commun. **178**, 852 (2008).

[22] J. Alwall et al., J. High Energy Phys. **09**, 028 (2007)

[23] M. Hentschinski, A. Sabio Vera, Phys. Rev. **D85**, 056006 (2012), G. Chachamis, M. Hentschinski, J. D. Madrigal, A. Sabio Vera, [arXiv: 1212.4992 [hep-ph]] (2012).

[24] V. Fadin, R. Fiore, A. Quartarolo, Phys. Rev. **D50**, 2265 (1994), Phys. Rev. **D50**, 5893 (1994), V. S. Fadin, R. Fiore, M. I. Kotsky, A. Papa, Phys. Rev. **D61**, 094005 (2000) V. S. Fadin, R. Fiore, A. Papa, Phys. Rev. **D63**, 034001 (2000).

Appendix

1: $RR \to gg$

$$
\begin{aligned}
A &= \frac{18}{a_1a_2b_1b_2s^2t^2u^2t_1t_2},\\
W_0 &= x_1x_2s^2tut_1t_2\big(x_1x_2(tu+t_1t_2)+(a_1b_2+a_2b_1)tu\big),\\
W_1 &= x_1x_2st_1t_2\bigg[t^2u\bigg(a_1b_2(a_2b_2+a_1x_2)(t_1+t_2)-a_2b_1(a_1b_1t_1+a_2b_2t_2)+\\
&+ \big(x_2(a_1^2b_2+a_2^2b_1)+a_1a_2(b_1-b_2)^2\big)u+x_1x_2a_1b_2t\bigg)\bigg]+\bigg[a_1\leftrightarrow a_2,b_1\leftrightarrow b_2,t\leftrightarrow u\bigg],\\
W_2 &= a_1a_2b_1b_2tu\bigg(x_1^2x_2^2\big[2(t_1+t_2)\big(t^2u+t_1t_2(s+u-t)\big)+tu\big((t_1-t_2)^2+t(u+2t)\big)\big]+\\
&+ x_1x_2tt_1t_2\big(4(x_1b_1+x_2a_2)(s+u)-(a_1b_1+a_2b_2)u\big)+\\
&+ tu\big(x_1^2b_2(2x_2t-b_1t_1)t_1+x_2^2a_1(2x_1t-a_2t_2t_2)\big)\bigg)+\bigg(a_1\leftrightarrow a_2,b_1\leftrightarrow b_2,t\leftrightarrow u\bigg),\\
W_3 &= x_1x_2a_1a_2b_1b_2\bigg[t^2u\bigg(2a_1b_2\big(x_1x_2(t_1+t_2)(2t-u-s)-(x_1b_2t_1+x_2a_1t_2)(u+s)\big)+\\
&+ \big[x_1t_1\big(2(a_1b_2^2+a_2b_1^2)+3x_1b_1b_2\big)+x_2t_2\big(2(a_1^2b_2+a_2^2b_1\big)+3a_1a_2x_2)\big]u+\\
&+ 4x_1x_2t\big((a_1b_2+a_2b_1)u+a_1b_2t\big)\bigg)\bigg]+\bigg[a_1\leftrightarrow a_2,b_1\leftrightarrow b_2,t\leftrightarrow u\bigg],\\
W_4 &= x_1^2x_2^2a_1a_2b_1b_2\bigg[t\bigg(a_1a_2b_1b_2u(t_1+t_2)(t-u-s)+(a_1b_2+a_2b_1)^2tu^2-\\
&- 2a_1b_2t(s+u)(2a_2b_1u-a_1b_2s)\bigg)\bigg]+\bigg[a_1\leftrightarrow a_2,b_1\leftrightarrow b_2,t\leftrightarrow u\bigg]. \qquad (35)
\end{aligned}
$$

2: $RR \to q\bar{q}$

$$
\begin{aligned}
A &= \frac{S}{3s^2t^2u^2t_1t_2},\\
W_0 &= 18x_1x_2st^2u^2t_1t_2,\\
W_1 &= tu\bigg(-18tu\big((x_1b_1t_1-a_1x_2t_2)+x_1x_2(u+t_2)\big)\big((x_1b_1t_1-a_1x_2t_2)-x_1x_2(t+t_1)\big)+\\
&+ x_1x_2s\big[9\big((t-u)(a_1b_2-a_2b_1)t_1t_2-x_1x_2stu\big)-x_1x_2s(t_1t_2-tu)\big]\bigg),\\
W_2 &= x_1x_2tu\big[9\big(2(x_1b_1t_1-x_2a_1t_2)-x_1x_2(t+t_1-u-t_2)\big)\times\\
&\times \big(2(a_2b_1-a_1b_2)tu-(a_1b_2t-a_2b_1u)s\big)-7x_1x_2s^2(a_2b_1u+a_1b_2t)\big],\\
W_3 &= -x_1^2x_2^2\big[18tu(a_2b_1-a_1b_2)\big((a_2b_1-a_1b_2)tu+(a_2b_1u-a_1b_2t)s\big)+\\
&+ 2s^2(4a_2^2b_1^2u^2+4a_1^2b_2^2t^2-a_1a_2b_1b_2tu)\big],\\
W_4 &= 0. \qquad (36)
\end{aligned}
$$

3: $QR \to qg$

$$
\begin{aligned}
A &= -\frac{8x_1}{9a_2b_1b_2st^2u^2t_2},\\
W_0 &= -9x_2t_2stu\big(x_2t_1t_2+(x_2+b_2)tu\big),\\
W_1 &= tu\bigg(-a_2b_1b_2tu\big[8\big(b_1(s+t)-b_2u\big)+x_2s\big]+\\
&+\big[9x_2^2\big(a_2(b_1-b_2)s^2+(a_2b_1+a_1b_2)st-a_1b_2tu\big)+\\
&+9x_2a_2u\big((b_1^2-2b_1b_2-b_2^2)s-b_1b_2u\big)+\\
&+x_2a_2b_1t\big((b_1-b_2)s+b_1t\big)+2a_2b_1tu(b_1^2+b_1b_2+4b_2^2)\big]t_2+\\
&+x_2\big((a_2b_1t+9a_2x_2s)(b_1-b_2)+9b_1b_2u(a_1-a_2)\big)t_2^2\bigg),\\
W_2 &= a_2b_1b_2x_2tu\bigg(9\big(a_1t(x_2s+b_2u)-a_2u(x_2s-b_2u)-2a_2b_1u(t+s)\big)+\\
&+b_1t(a_1t+a_2u)-2a_1b_2t(s+u)+\\
&+\Big[9\big(x_1x_2(s+u)+2a_1b_1u+x_2a_1(s-3u)\big)+(b_1x_1-2a_1b_2)t\Big]t_2\bigg),\\
W_3 &= a_2b_1b_2x_2^2\bigg(9\big[s\big(a_1^2b_2t^2-2a_2^2b_1u^2+a_1a_2ut(b_1-b_2)\big)+a_2tu^2(a_1b_2-a_2b_1)\big]-\\
&-t^2\big(u(a_1b_2-a_2b_1)+a_1b_2s\big)\bigg),\\
W_4 &= 0.
\end{aligned}
\tag{37}
$$

4: $QQ \to qq$

$$
\begin{aligned}
A &= \frac{64x_1x_2}{27a_1a_2b_1b_2t^2u^2},\\
W_0 &= x_1x_2st\big[t_1t(3a_2b_1-x_1b_2)+t_2t(3a_2b_1-x_2a_1)+t_1t_2(x_2a_2-x_1b_2)-x_1x_2t^2+\\
&+st\big(6(a_1b_1+a_2b_2)+5(2a_2b_1+a_1b_2)\big)\big],\\
W_1 &= t\big[t_1x_1a_2b_2\big(6b_1t(a_2b_1-a_1b_2)-x_2s(x_1b_1+a_2b_1-a_1b_2)\big)+\\
&+t_2x_2a_1b_1\big(6a_2t(a_2b_1-a_1b_2)-x_1s(x_2a_2+a_2b_1-a_1b_2)\big)+\\
&+6x_1x_2a_2b_1(a_2b_1-a_1b_2)t^2+x_1x_2a_2b_1s^2(a_2b_1-a_1b_2+6x_1x_2)+\\
&+x_1x_2st\big((a_1b_2-a_2b_1)^2+a_1b_2(a_1b_1+a_2b_2)-2a_2b_1(2a_2b_1+x_1b_2+x_2a_1)\big)\big],\\
W_2 &= x_1x_2a_2b_1\big(6t^2(a_2b_1-a_1b_2)^2+3x_1x_2a_2b_1s^2+st(x_1b_1+x_2a_2)(a_1b_2-a_2b_1)\big),\\
W_3 &= W_4 = 0.
\end{aligned}
\tag{38}
$$

5: $QQ' \to qq'$

$$A = \frac{64x_1x_2}{9a_2b_1t^2}, \qquad W_0 = 2t^2, \quad W_1 = 2a_2b_1t, \quad W_2 = a_2^2b_1^2, \quad W_3 = 0, \quad W_4 = 0. \tag{39}$$

6: $Q\bar{Q} \to q\bar{q}$

$$\begin{aligned}
A &= \frac{64}{27x_1x_2a_2b_1s^2t^2}, \\
W_0 &= x_1x_2st\big[t_1t(3a_2b_1 - x_1b_2) + t_2t(3a_2b_1 - x_2a_1) + t_1t_2(x_2a_2 - x_1b_2) - x_1x_2t^2 + \\
&+ st\big(6(a_1b_1 + a_2b_2) + 5(2a_2b_1 + a_1b_2)\big)\big], \\
W_1 &= t\big[t_1x_1a_2b_2\big(6b_1t(a_2b_1 - a_1b_2) - x_2s(x_1b_1 + a_2b_1 - a_1b_2)\big) + \\
&+ t_2x_2a_1b_1\big(6a_2t(a_2b_1 - a_1b_2) - x_1s(x_2a_2 + a_2b_1 - a_1b_2)\big) + \\
&+ 6x_1x_2a_2b_1(a_2b_1 - a_1b_2)t^2 + x_1x_2a_2b_1s^2(a_2b_1 - a_1b_2 + 6x_1x_2) + \\
&+ x_1x_2st\big((a_1b_2 - a_2b_1)^2 + a_1b_2(a_1b_1 + a_2b_2) - 2a_2b_1(2a_2b_1 + x_1b_2 + x_2a_1)\big)\big], \\
W_2 &= x_1x_2a_2b_1\big(6t^2(a_2b_1 - a_1b_2)^2 + 3x_1x_2a_2b_1s^2 + st(x_1b_1 + x_2a_2)(a_1b_2 - a_2b_1)\big), \\
W_3 &= W_4 = 0.
\end{aligned} \tag{40}$$

7: $Q\bar{Q} \to q'\bar{q}'$

$$\begin{aligned}
A &= \frac{64}{9x_1x_2s^2}, \\
W_0 &= -x_1x_2s(t+u), \\
W_1 &= 2\big(a_1^2b_1b_2(t_1+u) + a_1^2b_2^2u + a_1a_2b_1^2(t+t_2) + a_1a_2b_1b_2(t_1+t_2-s) + \\
&+ a_1a_2b_2^2(t_2+u) + a_2^2b_1^2t + a_2^2b_1b_2(t_1+t)\big), \\
W_2 &= 2x_1x_2(a_2b_1 - a_1b_2)^2, \\
W_3 &= W_4 = 0.
\end{aligned} \tag{41}$$

8: $Q\bar{Q} \to gg$

$$
\begin{aligned}
A &= \frac{1}{27x_1x_2Sa_1a_2b_1b_2s^2t^2u^2},\\
W_0 &= 2x_1x_2s^2tu\big[\big(x_1x_2-9(a_1b_2+a_2b_1)\big)(t+u)tu - x_1x_2t_1t_2(t_1+t_2)\big] + \big[a_1\leftrightarrow a_2, b_1\leftrightarrow b_2, t\leftrightarrow u\big],\\
W_1 &= -2x_1x_2stu\bigg(x_1x_2(a_1-a_2)(b_1-b_2)(t_1+t_2)t_1t_2 + 2t\big[x_1x_2(x_1b_2t_2^2+x_2a_1t_1^2) +\\
&+ t_1t_2\big((x_1x_2+x_1b_2+x_2a_1)(a_1b_1+a_2b_2)+(8a_2b_1-a_1b_2)(a_2b_1-a_1b_2)\big)\big] +\\
&+ x_1x_2\big(2x_1x_2-17(a_1b_2+a_2b_1)\big)(t_1+t_2)tu + 2\big(x_1^2(x_2+b_1)(b_2-8b_1) +\\
&+ x_2^2a_1(a_2-8a_1)+a_1b_1(25x_1x_2-72a_2b_2)\big)t^2u + 2t^2(x_1x_2-9a_2b_1)(x_1b_2t_2+x_2a_1t_1)\bigg) +\\
&+ \bigg(a_1\leftrightarrow a_2, b_1\leftrightarrow b_2, t\leftrightarrow u\bigg),\\
W_2 &= \bigg[-2tu\bigg(-x_1^2x_2^4a_1a_2(t_1+t_2)^2t_1 + 2x_1x_2a_1tt_1(t_1+t_2)\big[x_2^2\big(9a_1^2b_1-x_1(x_1x_2+a_1b_2)\big) +\\
&+ x_1(8b_1-b_2)\big(x_2^2(a_2-a_1)+a_2b_2^2\big)\big] +\\
&+ x_1tut_1\big(36x_1a_1a_2b_2^3(b_2-2x_2)+5a_1a_2x_1x_2^2b_2^2 - x_2^4a_2(x_1+a_1)(2a_1-7a_2) +\\
&+ 9x_2^2b_2(x_1^3b_2-2x_2a_1^3+4x_1^2x_2a_1) - 4x_1x_2^3b_2(a_1^2+4x_1^2)\big) + 2x_1x_2a_1t^2t_1\times\\
&\times \big[9a_2\big(b_2^2(3x_1b_1-2x_2a_1)-x_2^2b_2(x_1-3a_1)+x_2^3a_2\big) - 2x_1x_2b_2(a_1x_2+a_2b_2) - x_1x_2^3a_2\big] +\\
&+ x_1x_2t^2u\big(a_1^3b_2(7b_2^2+10b_1b_2-4b_1^2)+a_1^2a_2b_1(39b_2^2+30b_1b_2-2b_1^2) +\\
&+ 14a_1a_2^2b_1^2(x_2+2b_2)+8a_2^3b_1^3\big) + x_1x_2a_1b_2t^3\big(18a_2b_1(a_1x_2+x_1b_2)-x_1x_2(a_1b_1+x_1b_2)\big)\bigg) +\\
&+ \bigg(a_1\leftrightarrow b_2, a_2\leftrightarrow b_1, t_1\leftrightarrow t_2\bigg)\bigg] + \bigg[a_1\leftrightarrow a_2, b_1\leftrightarrow b_2, t\leftrightarrow u\bigg],\\
W_3 &= -4x_1x_2a_1a_2b_1b_2\bigg(t^2\big[8x_1x_2a_1b_2(s+u)^2 - u(s+u)\big((9a_2b_1+7a_1b_2)(a_1b_1+a_2b_2)+\\
&+ 2a_1b_2(17a_2b_1-a_1b_2)\big) + 2a_1u^2\big(4b_1(a_1b_2+a_2b_1)+b_2(13a_1b_2-5a_2b_1)\big)\big]\bigg) +\\
&+ \bigg(a_1\leftrightarrow a_2, b_1\leftrightarrow b_2, t\leftrightarrow u\bigg),\\
W_4 &= 0.
\end{aligned}
\tag{42}
$$

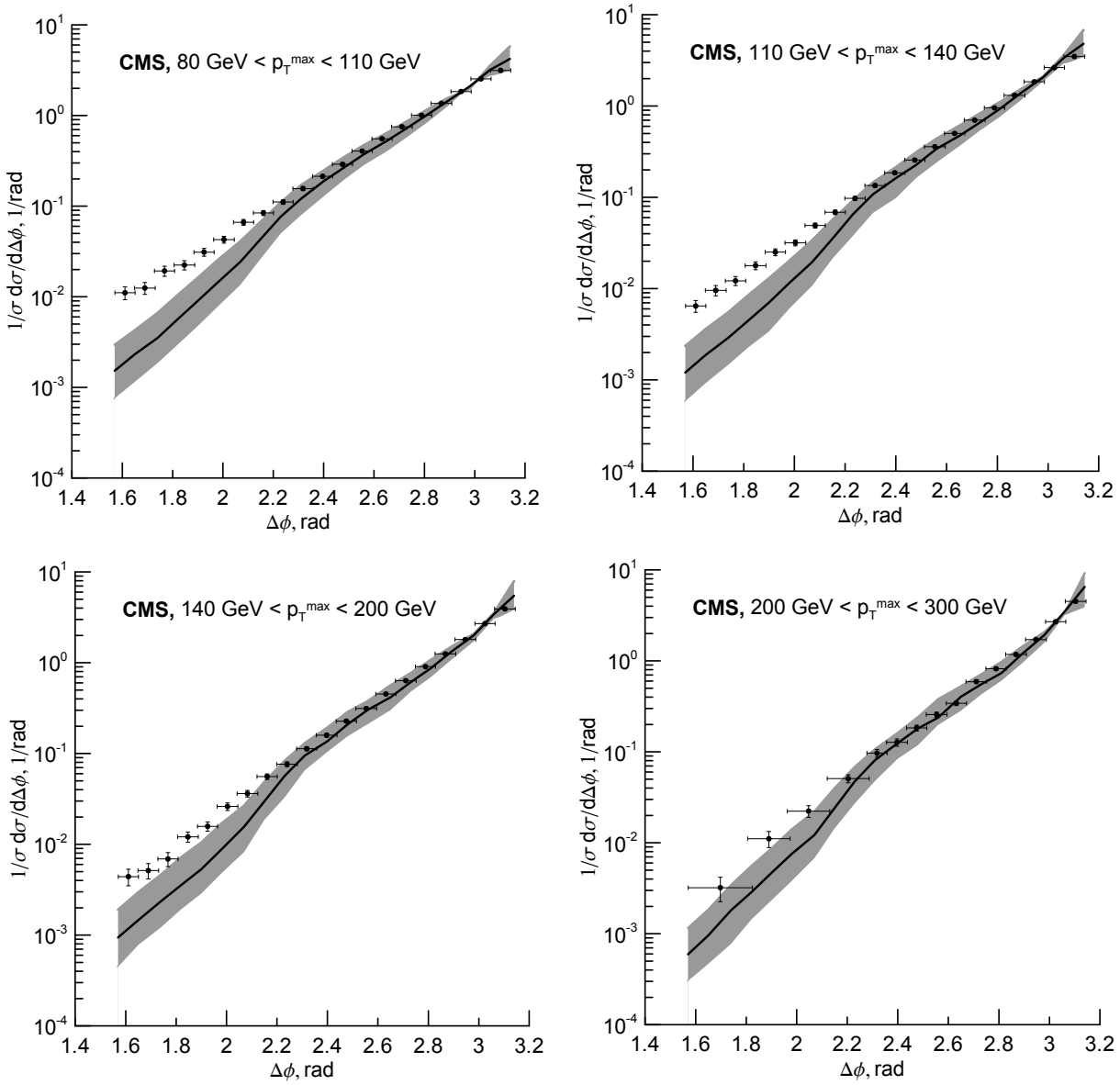

FIG. 1: Normalized $F(\Delta\phi)$ distributions in several p_T^{max} regions at the $\sqrt{S} = 7$ TeV, $|y| < 1.1$ and $p_T > 30$ GeV. The data are from the CMS Collaboration [2]. The curve corresponds to LO parton Reggeization approach.

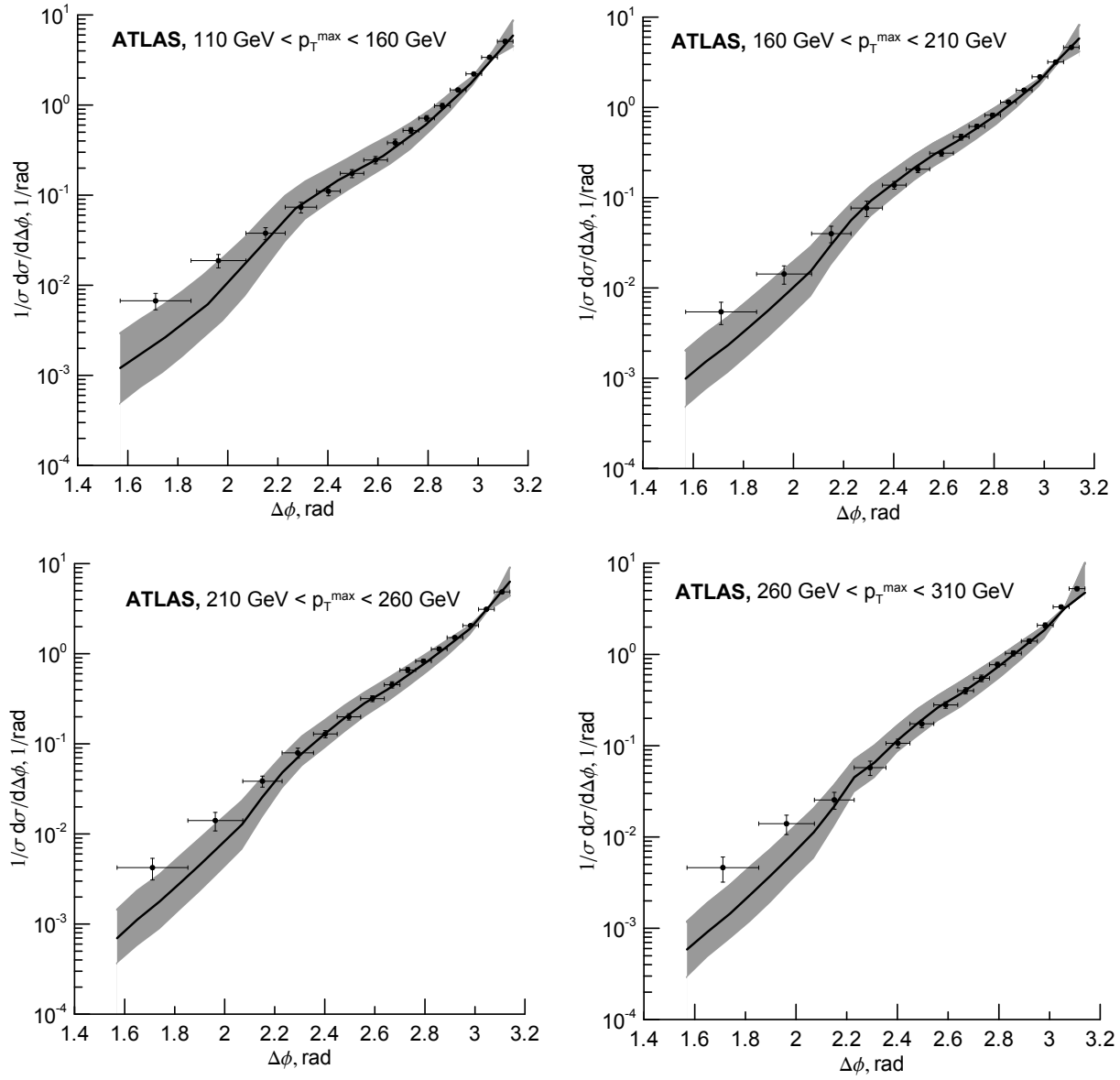

FIG. 2: Normalized $F(\Delta\phi)$ distributions in several p_T^{max} regions at the $\sqrt{S} = 7$ TeV, $|y| < 0.8$ and $p_T > 100$ GeV. The data are from the ATLAS Collaboration [3]. The curve corresponds to LO parton Reggeization approach.

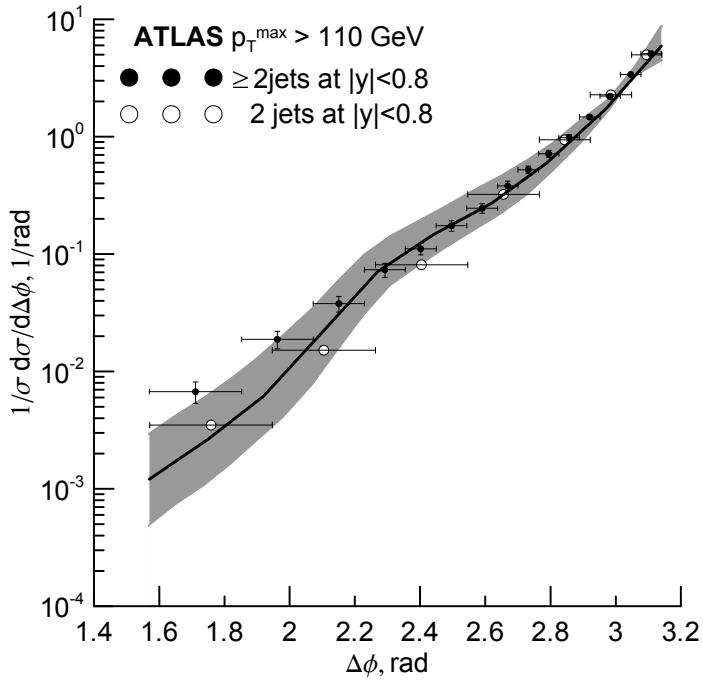

FIG. 3: Normalized $F(\Delta\phi)$ distribution for 2 (open circles) and $\geq$ 2 (black circles) jets with $p_T > 100$ GeV, $|y| < 0.8$, $p_T^{max} > 110$ GeV and $\sqrt{S} = 7$ TeV. The data are from the ATLAS Collaboration [3]. The curve corresponds to LO parton Reggeization approach.